THE ASTROPHYSICAL JOURNAL, 296:529–539, 1985 September 15

ACCRETION DISK OSCILLATIONS: A LOCAL ANALYSIS IN A DISK OF FINITE THICKNESS

B. W. CARROLL,[1] W. CABOT,[2] P. N. MCDERMOTT,[1] M. P. SAVEDOFF,[1] AND H. M. VAN HORN[1]

Received 1984 December 3; accepted 1985 March 14

ABSTRACT

Two types of oscillations are observed to occur in dwarf novae: "coherent" and "quasi-periodic" oscillations. These may be associated with the pulsation of the white dwarf or the accretion disk components of the dwarf nova. Here we utilize a local (short-wavelength) analysis to study the oscillation of a self-consistent, two-dimensional model of an accretion disk. The linearized equations describing adiabatic, inviscid, nonaxisymmetric oscillations are used to derive a fifth-order algebraic equation for the (complex) pulsation frequency of the disk. The solutions of this equation for various values of the wavevector $\boldsymbol{k}$ reveal that the disk is capable of supporting (1) a pair of high-frequency acoustic modes (p-modes); (2) a pair of intermediate-frequency modes which may share the characteristics of internal gravity waves (g-modes) and inertial waves; and (3) a mode associated with a dynamical instability (purely imaginary frequency). The role played by the shear in determining the stability or instability of these modes is also considered. Finally, we discuss the global oscillation frequencies of the disk.

Subject headings: stars: accretion — stars: dwarf novae — stars: pulsation

I. INTRODUCTION

Photometric observations of dwarf novae reveal two general types of pulsations (see Patterson 1981; Robinson and Nather 1979; Cordova and Mason 1982). There are the "dwarf nova oscillations" (DNO) and the "quasi-periodic oscillations" (QPO). The former type of oscillation is observed exclusively during outburst, while QPOs are sometimes seen during quiescence (J. Patterson, private communication).

The DNOs have relatively short periods, ranging from about 7 to 40 s, and amplitudes of about 0.002 mag. These "coherent" oscillations have rather high period stability, with $\dot{P} \approx 10^{-5}$. The DNOs usually display a single periodicity, and they exhibit a period-luminosity correlation: during rising light the period decreases, and during falling light it increases. In a period-luminosity diagram the periods trace out characteristic banana-shaped curves (Patterson 1981). A number of mechanisms to produce these oscillations have been discussed by Patterson (1981): orbiting blobs in the disk, white dwarf rotation, and nonradial white dwarf pulsations. Each of these encounters difficulties.

QPOs occur commonly in dwarf nova outbursts. The QPOs have longer periods than the DNOs, ranging from about 30 to 1000 s, and the pulsation amplitudes are 0.005 to 0.01 mag (Robinson and Nather 1979). They are characterized by broad humps in the power spectrum, which is indicative of their short coherence times of only a few cycles. The amplitudes can also change significantly on this same time scale. The lack of coherence of these oscillations argues against pulsations or rotation of the white dwarf. Robinson and Nather (1979) argue that the QPOs are produced in the accretion disk and specifically mention the possibility of "a traveling spiral pattern" or "oscillating rings."

These observations, in particular those of the QPOs, have prompted us to investigate the oscillation spectrum of dwarf nova accretion disks. The oscillations and dynamical stability of thin, non–self-gravitating accretion disks have been considered by numerous authors. We shall not attempt to review all the literature on this subject: instead we mention here only the work which is most pertinent to the present investigation.

Kato (1978) has studied stability against axially symmetric oscillations under a quasi-adiabatic, quasi-inviscid assumption in the local limit (which the wavelength λ is small compared to the disk radius R). The derived stability conditions depend strongly on the assumed arbitrary dependence of the viscosity on density and temperature. Van Horn, Wesemael, and Winget (1980) have considered vertical oscillations of disk annuli in which the radial coupling in the disk is neglected. The pulsation frequencies are found to be directly proportional to the rotational frequency Ω of the annulus. For disk parameters typical of dwarf novae, the oscillations have periods of ~ 20 s near the annulus with maximum luminosity. Livio and Shaviv (1981) consider stability against short-wavelength, axisymmetric perturbations in the z-direction. For α-model disks they find thermal instabilities with a rise time of $\sim 10/\alpha\Omega$ for $10^{-3} \lesssim \alpha \lesssim 1$ and pulsation frequencies of order Ω. Cox (1981) has derived, via Rayleigh's variational principle, an integral expression for adiabatic oscillations of an accretion disk. This expression has been applied to vertical oscillations of the disk with different vertical structures. The oscillation periods are invariably found to be comparable to the local Keplerian rotation period for the annuli considered. In a subsequent paper, Cox and Everson (1982) consider the effects of viscosity and nonadiabaticity on the vertical oscillation of an isothermal disk model. They find that if the QPOs are disk oscillations, and if they are damped mainly by viscosity, that the observed damping times imply an $\alpha \approx 1$. Cabot (1982) has given an extensive discussion of disk structure and stability. He has presented a local nonaxisymmetric, nonadiabatic stability analysis and has obtained a very general fifth-order dispersion relation for the complex frequency. Our analysis builds on the foundation provided by this work.

[1] Department of Physics and Astronomy and the C. E. K. Mees Observatory, University of Rochester.
[2] Goddard Institute for Space Studies.

Kato (1983) has examined the possibility of nonaxisymmetric (particularly one-armed, i.e., $m = 1$) oscillations. He has shown that under certain restrictive assumptions, one-armed, low-frequency waves are trapped in the central region of the disk. For these waves, he finds $\sigma \approx \Omega (c_s/\tilde{\omega}\Omega)^2$, where c_s is the adiabatic sound speed and $\tilde{\omega}$ is the cylindrical radius.

In a recent paper, Abramowicz *et al.* (1984) have considered the local stability for axisymmetric perturbations of thick accretion disks. They derive a dispersion relation for these oscillations, which is then analyzed in certain special, physically interesting cases; oscillations similar to p- and g-modes in stars were found for thick disks.

Our purpose here is to determine from a local analysis characteristic oscillation frequencies and modes of a thin accretion disk and to explore under what conditions the oscillations grow or decay. The equilibrium disk model utilized is a two-dimensional numerical model constructed by Cabot (1982). Our local perturbation analysis is in general nonaxisymmetric: it omits the effects of viscosity, nonadiabaticity, and meridional circulations.

The outline of this paper is as follows: § II is a description of the equilibrium disk model, § III is a discussion of the linearized equations of motion for the perturbation analysis, § IV involves specialization of the perturbation equations to the short wavelength limit and a derivation of a complex dispersion relation which is of fifth order in the frequency, in § V the solutions of the dispersion relation are presented for a number of interesting cases, and in § VI shear-induced instability is discussed. Finally, in § VII, we discuss possible implications for global oscillations, future plans, and an evaluation of the applicability of our results to both dwarf nova and quasi-periodic oscillation.

II. THE UNPERTURBED DISK MODEL

Steady axisymmetric αp models were calculated by Cabot (1982) in the spirit of the Pringle (1981) review. For cylindrical coordinates $\tilde{\omega}, \phi, z$, with corresponding velocities $v_{\tilde{\omega}}, v_\phi$, and v_z, we present the full time-dependent equations for later reference.

The momentum equation in component form is

$$\frac{D}{Dt} v_{\tilde{\omega}} = -\frac{1}{\rho}\frac{\partial p}{\partial \tilde{\omega}} + \Omega^2 \tilde{\omega} - \frac{\partial \Phi}{\partial \tilde{\omega}} + \frac{1}{\rho} \nabla \cdot \boldsymbol{T}_{\tilde{\omega}} - \frac{T_{\phi\phi}}{\rho \tilde{\omega}}, \tag{2.1}$$

$$\frac{D}{Dt} j = -\frac{1}{\rho}\frac{\partial p}{\partial \phi} - \frac{\partial \Phi}{\partial \phi} + \frac{1}{\rho} \nabla \cdot (\tilde{\omega} \boldsymbol{T}_\phi), \tag{2.2}$$

$$\frac{D}{Dt} v_z = -\frac{1}{\rho}\frac{\partial p}{\partial z} - \frac{\partial \Phi}{\partial z} + \frac{1}{\rho} \nabla \cdot \boldsymbol{T}_z; \tag{2.3}$$

the mass conservation equation is

$$\frac{D}{Dt} \rho = -\rho \nabla \cdot \boldsymbol{v}; \tag{2.4}$$

and the energy equation is

$$\rho T \frac{D}{Dt} S = \Theta_v - \nabla \cdot \boldsymbol{F}_r. \tag{2.5}$$

Here D/Dt represents the Stokes derivative, and we express v_ϕ in terms of the specific angular momentum j through

$$j = \tilde{\omega} v_\phi = \tilde{\omega}^2 \Omega. \tag{2.6}$$

We assume that self-gravity of the disk is negligible, so that the potential is

$$\Phi = -\frac{GM}{(\tilde{\omega}^2 + z^2)^{1/2}}. \tag{2.7}$$

In the spirit of the αp model, we introduce for the dissipative terms the expressions

$$\boldsymbol{T}_\phi = \alpha p_g \nabla\Omega / |\nabla\Omega|, \tag{2.8}$$

$$\boldsymbol{T}_{\tilde{\omega}} = \boldsymbol{T}_z = T_{\phi\phi} = 0. \tag{2.9}$$

We differ from some previous authors in two respects: we assume that the viscosity vanishes in vacuo (since $p_g \rightarrow 0$) and that the stress αp_g is divided between the $\hat{\phi}\hat{\tilde{\omega}}$ and $\hat{\phi}\hat{z}$ components in proportion to the shear $\nabla\Omega$. The pressure and density are assumed related by the equation of state

$$p = p_g + p_r = \frac{k}{\mu m_u} \rho T + \frac{1}{3} a T^4 \tag{2.10}$$

for fixed ionization and hence fixed μ. The consistent expression (up to a constant) for the entropy is

$$S = \frac{k}{\mu m_u} \ln (T^{3/2}/\rho) + \frac{4a}{3\rho} T^3. \tag{2.11}$$

In the energy equation (2.5) we express the viscous heat dissipation as

$$\Theta_v = \tilde{\omega}\nabla\Omega \cdot \boldsymbol{T}_\phi \,. \tag{2.12}$$

Lastly, the heat flux is evaluated in the diffusion approximation except for the surface layers which are represented by a gray plane parallel atmosphere. In the interior,

$$\boldsymbol{F}_r = -\frac{4ac}{3\kappa\rho} T^3 \nabla T \,. \tag{2.13}$$

We neglect both convection and conduction and represent the opacity by the Kramers-like approximation

$$\kappa = 0.4 \text{ cm}^2 \text{ g}^{-1} + 6.4 \times 10^{22} \text{ cm}^5 \text{ g}^{-2} \text{ K}^{3.5} \rho T^{-3.5} \,. \tag{2.14}$$

Thus at low densities, electron scattering predominates. These parameters approximate an ionized disk fairly well but are inadequate to represent regions with appreciable partially ionized material; in the latter regions, convection also is expected.

A steady-state solution of the equation set (e.g., with $\partial/\partial t = 0$) was obtained for $M = 1\ M_\odot$, $\dot{M} = 10^{17}$ g s^{-1}, and $\alpha = 0.4$. Details of the method of numerical solution and the difficult representation of the surface boundary conditions and gray atmosphere may be found in Cabot (1982). The solution begins with the construction of equilibrium vertical models for each annulus separately. These are then iterated to self-consistency with appropriate radial gradients and meridional circulations, and constant $\dot{M}$. The calculations show residuals in the five equilibrium equations which are limited by machine accuracy.

A surprising feature of the equilibrium disk model is that the nonbaroclinic solutions (since $dp/d\tilde{\omega} \neq 0$) imply an equatorial flow outward despite a net inflow of material. The outermost layer tabulated in our model is the one where $\tau = 0.2$; we define the height of this layer to be $z_{0.2}$, a function of $\tilde{\omega}$. The model values here, especially for the meridional velocities, are probably accurate only to $\tau = 1$. However, the thermodynamic variables of the model are self-consistent even near $\tau = 0.2$. For $\tilde{\omega} = 4.9 \times 10^9$ cm, the outward velocity near $z = 0$ is 2×10^4 cm s^{-1}, or $\sim 0.005 c_s$, where c_s is the local sound speed. The flow vanishes at $z = 6.6 \times 10^7$ cm or $0.3 z_{0.2}$ and reaches a minimum near $z = 2.2 \times 10^8$ cm ($\tau = 0.2$), where $v_{\tilde{\omega}} = 2.6 \times 10^5$ cm s^{-1} or $\sim 0.1 c_s$. The mass flux inward peaks at $z = 0.65 z_{0.2} = 1.3 \times 10^8$ cm. At all points, v_z is approximately 1.5 orders of magnitude smaller than $v_{\tilde{\omega}}$, and both are negligible compared to $v_\phi \approx 2.3 \times 10^8$ cm s^{-1}. We neglect these meridional velocities in our local analysis; they are always less than $0.1 c_s$ even in the tenuous atmosphere, where our numerical accuracy is most strained.

Upon vertical averaging, the structure of the equilibrium disk model closely resembles standard one-dimensional models. The importance of using a two-dimensional disk is that the vertical stratification allows modes of oscillation not found in vertically averaged models. This will be discussed below in §§ V and VII.

In Table 1 we present abbreviated samples of the tabular data used in our local analysis for the three heights and 10 radii selected for discussion. These are part of the approximately 160 × 90 representative model points available.

III. THE LINEARIZED EQUATIONS

The basic disk structure equations (2.1)–(2.4) may be linearized to produce four equations involving the Eulerian variations (e.g., f') of the pressure, the density, and the three components of the velocity field. Assuming, as usual, that all quantities f' vary as $e^{i(m\phi + \sigma t)}$, the linearized equations are:

$$i(\sigma + m\Omega)v'_{\tilde{\omega}} - 2\Omega v'_\phi = \frac{\rho'}{\rho^2}\frac{\partial}{\partial\tilde{\omega}} p - \frac{1}{\rho}\frac{\partial}{\partial\tilde{\omega}} p' \,, \tag{3.1}$$

$$i(\sigma + m\Omega)v'_\phi + \left(2\Omega + \tilde{\omega}\frac{\partial\Omega}{\partial\tilde{\omega}}\right)v'_{\tilde{\omega}} + \tilde{\omega}\frac{\partial\Omega}{\partial z} v'_z = -i\frac{m}{\tilde{\omega}}\frac{1}{\rho} p' \,, \tag{3.2}$$

$$i(\sigma + m\Omega)v'_z = \frac{\rho'}{\rho^2}\frac{\partial}{\partial z} p - \frac{1}{\rho}\frac{\partial}{\partial z} p' \,, \tag{3.3}$$

$$i(\sigma + m\Omega)\rho' + \left(\frac{\rho}{\tilde{\omega}} + \frac{\partial}{\partial\tilde{\omega}}\rho\right)v'_{\tilde{\omega}} + \rho\frac{\partial}{\partial\tilde{\omega}} v'_{\tilde{\omega}} + i\frac{m}{\tilde{\omega}}\rho v'_\phi + v'_z\frac{\partial}{\partial z}\rho + \rho\frac{\partial}{\partial z} v'_z = 0 \,. \tag{3.4}$$

Note, as mentioned in § II, that the meridional velocities $v_{\tilde{\omega}}$ and v_z in the equilibrium model have been neglected. The effects of viscosity on the oscillations have also been ignored.

Because the oscillations are assumed to be adiabatic (for simplicity), the energy equation (2.5) becomes

$$\frac{D}{Dt} p = c_s^2 \frac{D}{Dt}\rho \,,$$

where $c_s^2 = \Gamma_1 p/\rho$ is the adiabatic sound speed. Upon linearization this yields

$$i(\sigma + m\Omega)p' + v'_{\tilde{\omega}}\frac{\partial}{\partial\tilde{\omega}} p + v'_z\frac{\partial}{\partial z} p - c_s^2\left[i(\sigma + m\Omega)\rho' + v'_{\tilde{\omega}}\frac{\partial}{\partial\tilde{\omega}}\rho + v'_z\frac{\partial}{\partial z}\rho\right] = 0 \,. \tag{3.5}$$

Equations (3.1)–(3.5) describe the adiabatic, inviscid oscillation of the accretion disk.

IV. THE LOCAL ANALYSIS

The solution of the linearized equations is hampered by the appearance of both $\tilde{\omega}$ and z-derivatives of the perturbed quantities f'. In the case of stellar pulsation, a separation of variables can be found that leaves only radial derivatives in the pulsation

TABLE 1

EQUILIBRIUM MODEL[a]

$\tilde{\omega}$	z	p	ρ	Ω	$N_{\tilde{\omega}}$	N_z	c_s
"Equatorial" Points ($z/z_{0.2} \approx 2 \times 10^{-4}$)							
5.10E+08...	5.11E+03	2.28E+09	3.75E−05	9.99E−01	1.02E−02	2.06E−04	1.01E+07
8.53E+08...	8.53E+03	6.03E+08	1.53E−05	4.63E−01	5.30E−03	9.53E−05	8.09E+06
1.42E+09...	1.42E+04	1.59E+08	6.18E−06	2.14E−01	2.74E−03	4.34E−05	6.55E+06
2.38E+09...	2.38E+04	4.18E+07	2.46E−06	9.93E−02	1.40E−03	1.96E−05	5.33E+06
3.97E+09...	3.97E+04	1.10E+07	9.64E−07	4.60E−02	7.04E−04	8.72E−06	4.35E+06
6.63E+09...	6.64E+04	2.87E+06	3.76E−07	2.13E−02	3.53E−04	3.86E−06	3.57E+06
1.10E+10...	1.10E+05	7.58E+05	1.47E−07	9.95E−03	1.77E−04	1.71E−06	2.93E+06
1.80E+10...	1.80E+05	2.11E+05	5.93E−08	4.78E−03	9.13E−05	7.81E−07	2.44E+06
2.93E+10...	2.93E+05	5.87E+04	2.39E−08	2.30E−03	4.69E−05	3.55E−07	2.02E+06
4.76E+10...	4.77E+05	1.63E+04	9.61E−09	1.11E−03	2.40E−05	1.62E−07	1.68E+06
"Intermediate" Points ($z/z_{0.2} \approx 5 \times 10^{-2}$)							
5.10E+08...	1.20E+06	2.25E+09	3.71E−05	9.99E−01	1.00E−02	4.87E−02	1.00E+07
8.53E+08...	2.01E+06	5.97E+08	1.52E−05	4.63E−01	5.23E−03	2.25E−02	8.08E+06
1.42E+09...	3.35E+06	1.58E+08	6.14E−06	2.14E−01	2.71E−03	1.02E−02	6.54E+06
2.38E+09...	5.60E+06	4.15E+07	2.44E−06	9.93E−02	1.38E−03	4.61E−03	5.32E+06
3.97E+09...	9.35E+06	1.09E+07	9.59E−07	4.60E−02	6.98E−04	2.06E−03	4.35E+06
6.63E+09...	1.56E+07	2.85E+06	3.74E−07	2.13E−02	3.50E−04	9.09E−04	3.56E+06
1.10E+10...	2.59E+07	7.54E+05	1.46E−07	9.95E−03	1.76E−04	4.03E−04	2.93E+06
1.80E+10...	4.23E+07	2.10E+05	5.90E−08	4.78E−03	9.07E−05	1.84E−04	2.43E+06
2.93E+10...	6.88E+07	5.84E+04	2.38E−08	2.30E−03	4.66E−05	8.37E−05	2.02E+06
4.76E+10...	1.12E+08	1.63E+04	9.58E−09	1.11E−03	2.39E−05	3.80E−05	1.68E+06
"Surface" Points ($z/z_{0.2} \approx 1$)							
5.10E+08...	1.84E+07	1.53E+07	7.91E−07	9.98E−01	8.26E−02	2.34E+00	5.67E+06
8.53E+08...	3.20E+07	4.24E+06	3.30E−07	4.63E−01	4.01E−02	1.08E+00	4.62E+06
1.42E+09...	5.59E+07	1.18E+06	1.37E−07	2.14E−01	1.94E−02	4.97E−01	3.78E+06
2.38E+09...	9.81E+07	3.28E+05	5.68E−08	9.93E−02	9.43E−03	2.28E−01	3.10E+06
3.97E+09...	1.73E+08	9.16E+04	2.35E−08	4.60E−02	4.56E−03	1.05E−01	2.55E+06
6.63E+09...	3.05E+08	2.51E+04	9.51E−09	2.13E−02	2.21E−03	4.80E−02	2.10E+06
1.10E+10...	5.36E+08	7.13E+03	3.95E−09	9.94E−03	1.07E−03	2.20E−02	1.73E+06
1.80E+10...	9.21E+08	2.10E+03	1.68E−09	4.78E−03	5.37E−04	1.04E−02	1.44E+06
2.93E+10...	1.59E+09	6.20E+02	7.13E−10	2.30E−03	2.68E−04	4.92E−03	1.20E+06
4.76E+10...	2.73E+09	1.89E+02	3.12E−10	1.11E−03	1.31E−04	2.30E−03	1.01E+06

[a] $\Gamma_1 = 5/3$ for all model points. Units are cgs.

equations. However, in the complicated geometry of our accretion disk we have been unable to find an exact separation of variables. We have therefore elected to carry out a local (short-wavelength) analysis of the linearized equations. Such an analysis reveals the range of frequencies and modes of oscillation that the accretion disk is capable of supporting. It allows an investigation of the stability of the disk in the short-wavelength limit.

In our local analysis, all perturbed quantities f' take the same space and time dependence, viz.,

$$f' = f_0 \, e^{i(k_{\tilde{\omega}}\tilde{\omega} + m\phi + k_z z + \sigma t)} , \tag{4.1}$$

where f_0 is a constant. Thus, all variables describing the equilibrium disk take on their local (constant) values. Under these conditions, the linearized equations (3.1)–(3.5) become five algebraic equations, which may be solved for $\Sigma = \sigma + m\Omega$, the pulsation frequency seen in the (local) reference frame corotating with the disk. In matrix form, these equations are

$$\begin{pmatrix} i\Sigma & \left(\frac{1}{\rho}\frac{\partial \rho}{\partial \tilde{\omega}} + ik_{\tilde{\omega}}\right)c_s & imc_s & \left(\frac{1}{\rho}\frac{\partial \rho}{\partial z} + ik_z\right)c_s & 0 \\ -\frac{1}{\rho}\frac{\partial p}{\partial \tilde{\omega}} & i\Sigma c_s & -2\Omega c_s & 0 & ik_{\tilde{\omega}}\frac{p}{\rho} \\ 0 & \left(2\Omega + \tilde{\omega}\frac{\partial \Omega}{\partial \tilde{\omega}}\right)c_s & i\Sigma c_s & \tilde{\omega}\frac{\partial \Omega}{\partial z}c_s & i\frac{m}{\tilde{\omega}}\frac{p}{\rho} \\ -\frac{1}{\rho}\frac{\partial p}{\partial z} & 0 & 0 & i\Sigma c_s & ik_z\frac{p}{\rho} \\ -i\Sigma\Gamma_1 & \left(\frac{1}{p}\frac{\partial p}{\partial \tilde{\omega}} - \frac{\Gamma_1}{\rho}\frac{\partial \rho}{\partial \tilde{\omega}}\right)c_s & 0 & \left(\frac{1}{p}\frac{\partial p}{\partial z} - \frac{\Gamma_1}{\rho}\frac{\partial \rho}{\partial z}\right)c_s & i\Sigma \end{pmatrix} \begin{pmatrix} \frac{\rho'}{\rho} \\ \frac{v'_{\tilde{\omega}}}{c_s} \\ \frac{v'_{\phi}}{c_s} \\ \frac{v'_z}{c_s} \\ \frac{p'}{p} \end{pmatrix} = 0 . \tag{4.2}$$

(We have neglected the "curvature term" $\rho/\tilde{\omega}$ in equation (3.4), as is appropriate for a short-wavelength analysis; cf. § 3.1 of Cabot 1982.)

Matrix equation (4.2) agrees with equation (3.37) of Cabot (1982). However, Cabot has retained the viscous, nonadiabatic, and meridional circulation terms neglected in our analysis. Abramowicz *et al.* (1984) consider only axisymmetric oscillations; they have also retained the meridional circulation terms, as well as the "geometrical term" mentioned above. With the neglect of these terms, their equation (3.6) agrees with our (4.2) with $m = 0$.

For a nontrivial solution, the determinant of the 5 × 5 matrix must vanish. This requirement leads to a fifth-order equation for the (corotating) frequency Σ:

$$\Sigma^5 - \Sigma^3\left(H_{\tilde{\omega}}^2 + N_{\tilde{\omega}}^2 + N_z^2 + S^2 + \frac{g^2}{c_z^2}\right) + \Sigma^2\left[\frac{m}{\tilde{\omega}}\left(\tilde{\omega}\frac{\partial\Omega}{\partial\tilde{\omega}}g_{\tilde{\omega}} + \tilde{\omega}\frac{\partial\Omega}{\partial z}g_z\right) + 4\Omega\frac{m}{\tilde{\omega}}g_{\tilde{\omega}} - ic_s^2\frac{m}{\tilde{\omega}}\left(k_{\tilde{\omega}}\tilde{\omega}\frac{\partial\Omega}{\partial\tilde{\omega}} + k_z\tilde{\omega}\frac{\partial\Omega}{\partial z}\right)\right]$$
$$+ \sum\left[c_s^2\left(\frac{m^2}{\tilde{\omega}^2} + k_z^2\right)N_{\tilde{\omega}}^2 + c_s^2\left(k_{\tilde{\omega}}^2 + \frac{m^2}{\tilde{\omega}^2}\right)N_z^2 - c_s^2 k_{\tilde{\omega}} k_z(g_{\tilde{\omega}} A_z + g_z A_{\tilde{\omega}}) + c_s^2 k_z^2 H_{\tilde{\omega}}^2 - c_s^2 k_{\tilde{\omega}} k_z H_z^2 + g_z\left(\frac{1}{\rho}\frac{\partial\rho}{\partial z}H_{\tilde{\omega}}^2 - \frac{1}{\rho}\frac{\partial\rho}{\partial\tilde{\omega}}H_z^2\right)\right]$$
$$+ \left\{2\Omega\frac{m}{\tilde{\omega}}g_z H_z^2 + ic_s^2\left[2\Omega\frac{m}{\tilde{\omega}}k_z H_z^2 - \frac{m}{\tilde{\omega}}(k_{\tilde{\omega}} g_z - k_z g_{\tilde{\omega}})\left(\tilde{\omega}\frac{\partial\Omega}{\partial z}A_{\tilde{\omega}} - \tilde{\omega}\frac{\partial\Omega}{\partial\tilde{\omega}}A_z\right)\right]\right\} = 0 . \quad (4.3)$$

In this equation, $g_{\tilde{\omega}}$ and g_z are the components of the "effective gravity" $\boldsymbol{g}$:

$$\boldsymbol{g} = \Omega^2\tilde{\omega}\hat{\tilde{\omega}} - \nabla\Phi = \frac{1}{\rho}\nabla p . \quad (4.4)$$

$N_{\tilde{\omega}}^2$ and N_z^2 are the "components" of N^2, the square of the Brunt-Väisälä frequency:

$$N^2 = N_{\tilde{\omega}}^2 + N_z^2 = \boldsymbol{g}\cdot\boldsymbol{A} , \quad (4.5)$$

where

$$\boldsymbol{A} = \nabla \ln \rho - \frac{1}{\Gamma_1}\nabla \ln p \quad (4.5a)$$

is the vector generalization of the Schwarzschild convective stability factor. The Brunt-Väisälä frequency is the characteristic frequency associated with internal gravity waves in a stratified fluid.

The square of the "Solberg-Hoiland frequency" is the magnitude of the vector

$$H_{\tilde{\omega}}^2\hat{\tilde{\omega}} + H_z^2\hat{z} = (\tilde{\omega})^{-3}\nabla(\tilde{\omega}^4\Omega^2) \quad (4.6)$$

(Tassoul 1978; Cabot 1982). The Solberg-Hoiland frequency is the characteristic frequency associated with inertial waves in a rotating fluid. (For a Keplerian orbit, $H_{\tilde{\omega}}^2 = \Omega^2$; $H_z^2 \neq 0$ as a result of the nonbaroclinic structure of the equlibrium disk model.) Finally, S^2 is the square of the acoustic frequency for sound waves:

$$S^2 = c_s^2 k^2 = c_s^2(k_{\tilde{\omega}}^2 + m^2/\tilde{\omega}^2 + k_z^2) . \quad (4.7)$$

Thus the quintic equation contains a variety of characteristic frequencies corresponding to various sorts of wave phenomena.

V. SOLUTIONS OF THE QUINTIC EQUATION

The quintic equation (4.3) for the oscillation frequency (as viewed from the local corotating reference frame) was solved numerically for several positions in the disk model and orientations of the wave vector $\boldsymbol{k}$, $\boldsymbol{k} = k_{\tilde{\omega}}\hat{\tilde{\omega}} + m/\tilde{\omega}\hat{\phi} + k_z\hat{z}$. In all cases to be discussed in §§ V and VI, the magnitude of the wave vector was chosen to satisfy $|\boldsymbol{k}|\tilde{\omega} = 10^5$. For this large value of the wave vector, S is the dominant characteristic frequency at all points in the disk model. The numerical solution was obtained by using the IMSL routine ZCPOLY. Once the values of Σ were determined for a given model point and orientation of $\boldsymbol{k}$, the eigenvector (ρ'/ρ, $v'_{\tilde{\omega}}/c_s$, v'_ϕ/c_s, v'_z/c_s, p'/p) was calculated by using the IMSL routine LEQTIC. (The matrix eq. [4.2] is homogeneous; thus the eigenvector is subject to an arbitrary normalization. As a result, only four of the five linearized equations need be used to determine the eigenvector. The remaining equation was used as a check on the consistency of the solution. This equation was always satisfied to within machine accuracy.)

It is instructive to examine first the cases for which $\boldsymbol{k}$ is directed parallel to the $\tilde{\omega}$-, ϕ-, and z-axes. For these orientations, the frequency Σ is real; this offers the opportunity to examine relatively simple modes of oscillation. This was done for a choice of ten radial model points, equally spaced in log $\tilde{\omega}$, and two vertical model points: one virtually on the equator, at $z/z_{0.2} \approx 2 \times 10^{-4}$; the other near the surface of the disk, at $z \approx z_{0.2}$. (See Table 1; note that the vertical height z increases with $\tilde{\omega}$ in such a way that $z/\tilde{\omega}$ is approximately constant.)

The numerical solutions for Σ may be compared with approximate solutions of the quintic equation (4.3). Keeping only the leading order terms in k for each coefficient reduces the quintic to a quartic equation; the fifth root of the quintic is thus identically zero for this approximation.

For $\boldsymbol{k}$ oriented in the radial ($\tilde{\omega}$) direction, the numerical results (see Figs. 1, 2) show that $\Sigma = \pm S$ and $\pm N_z$, in agreement with the analytic result:

$$\Sigma^2 = \tfrac{1}{2}(S^2 \pm \sqrt{S^4 - 4S^2N_z^2}) \approx S^2, N_z^2 , \quad (5.1)$$

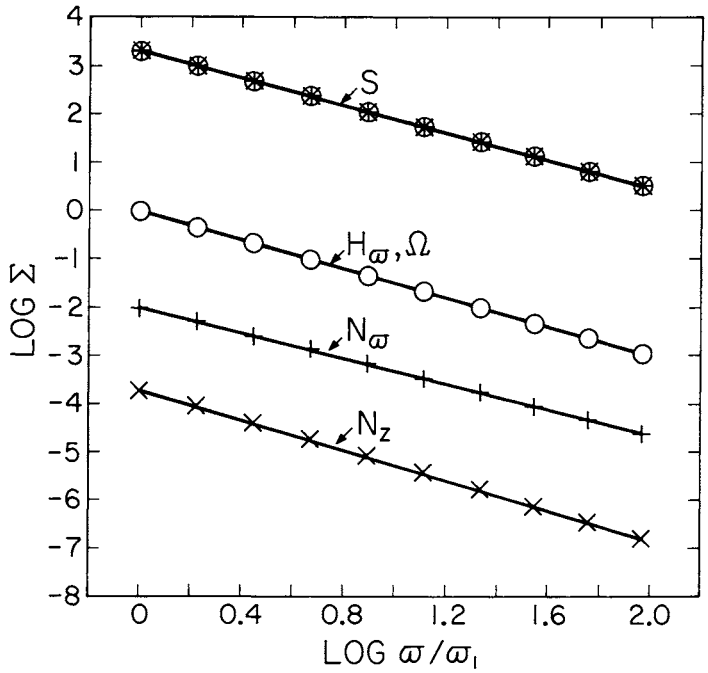

FIG. 1.—Characteristic frequencies and solutions Σ of the quintic equation (4.3) evaluated at ten "equatorial" model points. Crosses indicate $\boldsymbol{k} = |k|\hat{\tilde{\omega}}$; plusses indicate $\boldsymbol{k} = |k|\hat{\phi}$; circles indicate $\boldsymbol{k} = |k|\hat{z}$. All frequencies are in units of rad s^{-1}.

since $S^2 \gg N_z^2$ for all points in the disk model. The direction of $\boldsymbol{v}'$ is longitudinal (in the $\tilde{\omega}$-direction) for $\Sigma = \pm S$, as expected for sound waves, and transverse (in the z-direction) for $\Sigma = \pm N_z$, as expected for internal gravity waves. For $\boldsymbol{k}$ in the $\tilde{\omega}$-direction, the internal gravity wave oscillations "see" only the vertical stratification of the disk.

For $\boldsymbol{k}$ oriented in the azimuthal (ϕ) direction, the numerical results show that $\Sigma = \pm S$ and $\pm N$ (where N is defined by eq. [4.5]), in agreement with the analytic results:

$$\Sigma^2 = \tfrac{1}{2}[S^2 \pm \sqrt{S^4 - 4S^2(N_{\tilde{\omega}}^2 + N_z^2)}] \approx S^2, N^2 . \tag{5.2}$$

For the lower model point, $N \approx N_{\tilde{\omega}}$, while $N \approx N_z$ for the higher point. As before, $\boldsymbol{v}'$ is longitudinal (in the ϕ-direction) for $\Sigma = \pm S$. As expected for internal gravity waves, $\boldsymbol{v}'$ is transverse (in the $\tilde{\omega}$-direction for the lower point, and essentially in the z-direction for the higher point) for $\Sigma = \pm N$. For $\boldsymbol{k}$ in the ϕ-direction, the oscillations "see" both the radial and vertical stratification of the disk.

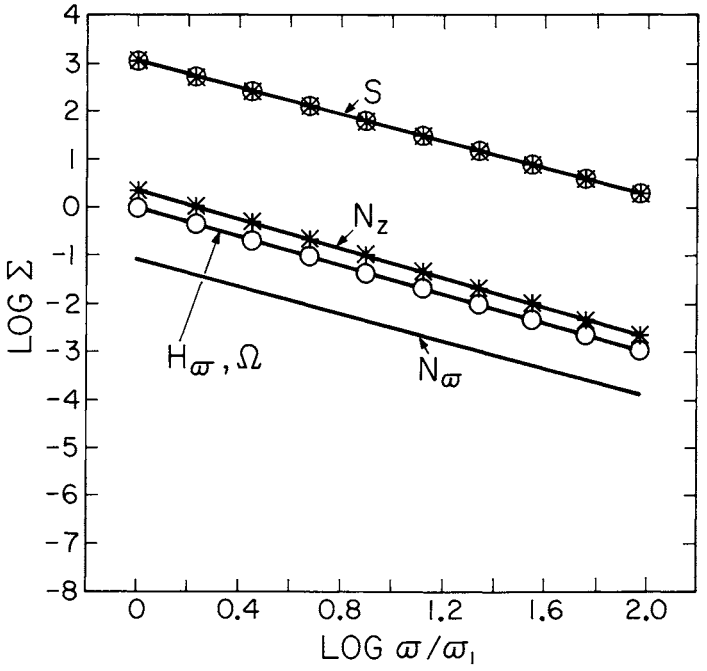

FIG. 2.—Characteristic frequencies and solutions Σ of the quintic equation (4.3) evaluated at ten "surface" model points; same notation as Fig. 1

Finally, for $\boldsymbol{k}$ oriented in the vertical (z) direction, the numerical results show that $\Sigma = \pm S$ and $\pm H_{\tilde{\omega}}$, in agreement with the analytic result:

$$\Sigma^2 = \tfrac{1}{2}[S^2 \pm \sqrt{S^4 - 4S^2(N_{\tilde{\omega}}^2 + H_{\tilde{\omega}}^2)}] \approx S^2, H_{\tilde{\omega}}^2 , \tag{5.3}$$

since $S^2 \gg H_{\tilde{\omega}}^2 \gg N_{\tilde{\omega}}^2$ for all points in the disk model. Again, $\boldsymbol{v}'$ is longitudinal (in the z-direction) for $\Sigma = \pm S$, while for $\Sigma = \pm H_{\tilde{\omega}}$, $\boldsymbol{v}'$ is transverse (as expected for an inertial wave) with $v'_\phi = \pm \frac{1}{2} i v'_{\tilde{\omega}}$. The mass elements thus librate around their equilibrium positions with frequency $H_{\tilde{\omega}}$. The effect of rotation dominates the effect of the stratification for $\boldsymbol{k}$ in the vertical direction.

The above cases illustrate the disk's ability to support sound, internal gravity, and inertial waves. Although the results are qualitatively the same for different radii, they can vary with height in the disk. In addition, the solution for vertical $\boldsymbol{k}$ indicates that waves of mixed type may occur.

In general, the solutions Σ of the full quintic equation (4.3) are usually complex, corresponding to exponentially growing [$Im(\Sigma) < 0$] or decaying [$Im(\Sigma) > 0$] pulsation amplitudes. As seen below in § VI, the direction of maximum stability or instability, for fixed $|\boldsymbol{k}|$ and k_z, usually occurs for the case $|k_{\tilde{\omega}}| = |m/\tilde{\omega}|$. Thus we will next investigate the special case $k_{\tilde{\omega}} = m/\tilde{\omega}$ with $|\boldsymbol{k}|\tilde{\omega} = 10^5$ as before. The results are independent of the sign of k_z. However, in those quadrants where $k_{\tilde{\omega}} m/\tilde{\omega} < 0$, $Im(\Sigma)$ should be replaced by $-Im(\Sigma)$ for each of the five solutions; the corresponding real parts are unchanged. While these are not exact symmetries of the quintic equation (4.3), they are adequate for the short-wavelength approximation, provided $|\boldsymbol{k}|$ is sufficiently large that the real parts of the coefficients Σ^2 and Σ^0 can be neglected.

Because the results are (qualitatively) independent of the radial position in the disk, only one radial point need be considered. We have chosen a point at $\log(\tilde{\omega}/\tilde{\omega}_1) = 0.668$, where $\tilde{\omega}_1$ is the inner radius of the disk model. The numerical solution of the quintic equation was determined, at this radial point, for the two vertical points used above. Figures 3–7 show, for each combination of radial and vertical points, the real and imaginary parts of Σ plotted as a function of $\theta = \sin^{-1}(k_z/|\boldsymbol{k}|)$. We note that, near $\theta = 0°$ and $\theta = 90°$, a local analysis may not be strictly valid because some components of $\boldsymbol{k}$ become vanishingly small.

Only the numerical results will be described in the remainder of this section; an interpretation of the physical principles underlying the results will be deferred to § VI.

At both model points selected, the sound wave frequency ($Re(\Sigma) = \pm S$) is independent of the orientation of $\boldsymbol{k}$. These oscillations are stable (unstable) when $k_{\tilde{\omega}} m/\tilde{\omega} < 0$ (> 0), with maximum stability or instability occurring when $|k_{\tilde{\omega}}| = |m/\tilde{\omega}|$ and $k_z = 0$. For these orientations of $\boldsymbol{k}$, $|Im(\Sigma)| = 3\Omega/8$. As the latitude θ increases from 0° to 90°, $|Im(\Sigma)|$ decreases smoothly to zero.

The behavior of the remaining three roots of the quintic equation varies with the height in the disk. For the "equatorial" model point, just off the equatorial plane of the disk, one of the roots is effectively zero. The other two solutions fall into two categories; for both, in contrast to the acoustic solutions, the oscillations are stable (unstable) when $k_{\tilde{\omega}} m/\tilde{\omega} > 0$ (< 0). Examination of the eigenvector shows that the velocity components are all in phase and perpendicular to $\boldsymbol{k}$.

If $\theta < 19°$, $Re(\Sigma) \approx 0$, as $\Sigma \ll H_{\tilde{\omega}}$, Ω, and N. For one solution, $Im(\Sigma) = 0$ when $\theta = 0°$, while for the other, $|Im(\Sigma)| = 3\Omega/4$ when $\theta = 0°$. As θ increases from 0° to 19°, the two solutions converge to $|Im(\Sigma)| \approx \Omega/3$. Thus, for $k_{\tilde{\omega}} m/\tilde{\omega} < 0$, the region $0° \leq \theta < 19°$ corresponds to a region of dynamical instability, with a growth rate given by the larger of the two imaginary roots.

If $\theta > 19°$, near the equatorial plane of the disk, these solutions correspond to secularly growing or damped oscillations, with the effect of rotation dominating the effect of stratification in determining the pulsation frequency. As θ increases from $\theta \approx 19°$ to $\theta = 90°$, $|Re(\Sigma)|$ increases from zero to Ω; also, $|Im(\Sigma)|$ decreases smoothly to zero. In fact, $|Im(\Sigma)|$ is the same as for the sound waves in this range of θ, although the signs are opposite. These oscillations are stable (unstable) when $k_{\tilde{\omega}} m/\tilde{\omega} > 0$ (< 0), with maximum stability or instability occurring at at $\theta \approx 19°$ (in the region under consideration), at the border of the region of dynamical instability.

For the "surface" model point, near the surface of the disk, all three of the remaining roots of the quintic equation are nonzero. One of these roots is purely imaginary, and this represents a dynamical instability (for $k_{\tilde{\omega}} m/\tilde{\omega} < 0$). For this root and model point, $|Im(\Sigma)|$ attains its maximum value, $3\Omega/4$, for $k_z = 0$; as θ goes from 0° to 90°, $|Im(\Sigma)|$ approaches zero. For the other two roots, $|Re(\Sigma)| = N_z$ when $\theta = 0°$ and decreases to $|Re(\Sigma)| = \Omega$ as θ approaches 90°. Thus, in determining the frequency of oscillation, the effect of stratification dominates for small values of θ ($\boldsymbol{k} \approx$ horizontal), while rotation is more important for larger values of θ ($\boldsymbol{k} \approx$ vertical). $Im(\Sigma)$ is zero when $\theta = 0°$ and $\theta = 90°$ but achieves a maximum value of $|Im(\Sigma)| = 0.14\Omega$ when $\theta \approx 59°$. The oscillations are stable (unstable) when $k_{\tilde{\omega}} m/\tilde{\omega} < 0$ (> 0).

These examples reveal the ability of the disk to support complicated modes of oscillation, encompassing instances of dynamical instability and competition between the effects of stratification and rotation in determining the frequency of oscillation of the accretion disk. Some of the physical principles underlying these results will be examined in the next section.

VI. INTERPRETATION

The previous numerical results can be understood qualitatively for simplified equations available in certain limits. For example, when Σ is much larger in absolute value than any of the characteristic frequencies $H_{\tilde{\omega}}$, $N_{\tilde{\omega}}$, and N_z, then quintic equation (4.3) reduces to

$$\Sigma^3 - \Sigma S^2 - iL = 0 , \tag{6.1}$$

where

$$L = c_s^2 k_{\tilde{\omega}} \frac{m}{\tilde{\omega}} \tilde{\omega} \frac{\partial \Omega}{\partial \tilde{\omega}} . \tag{6.2}$$

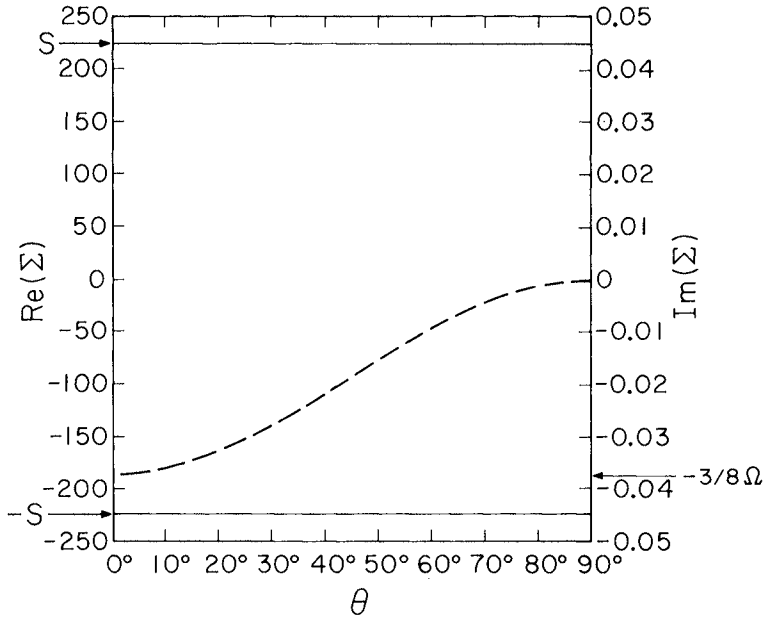

FIG. 3

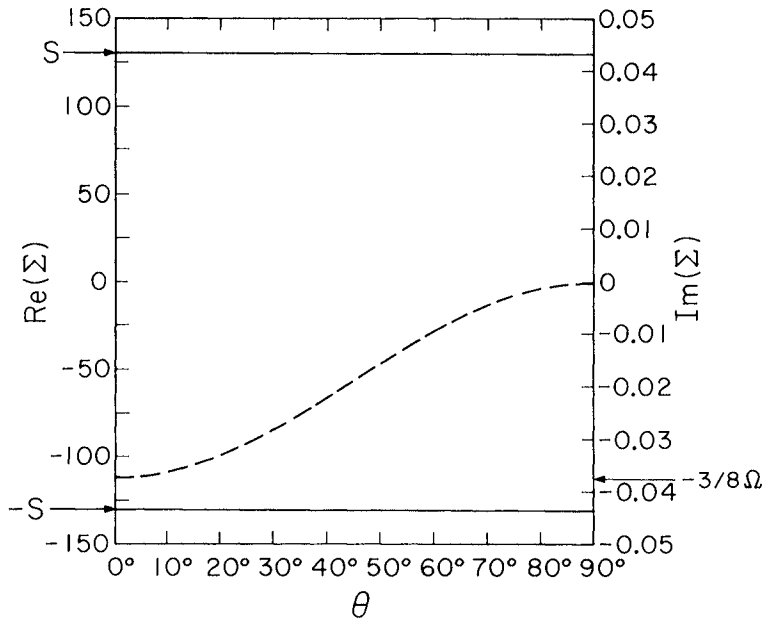

FIG. 4

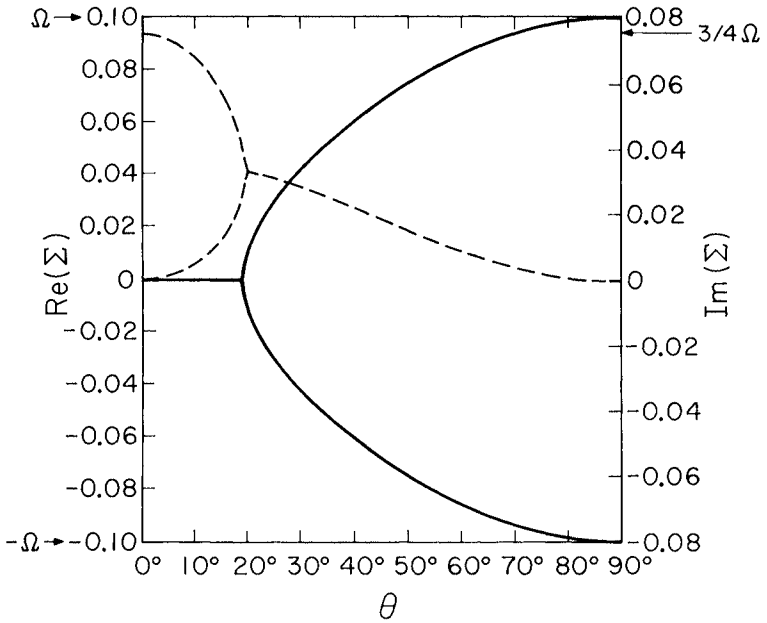

FIG. 5

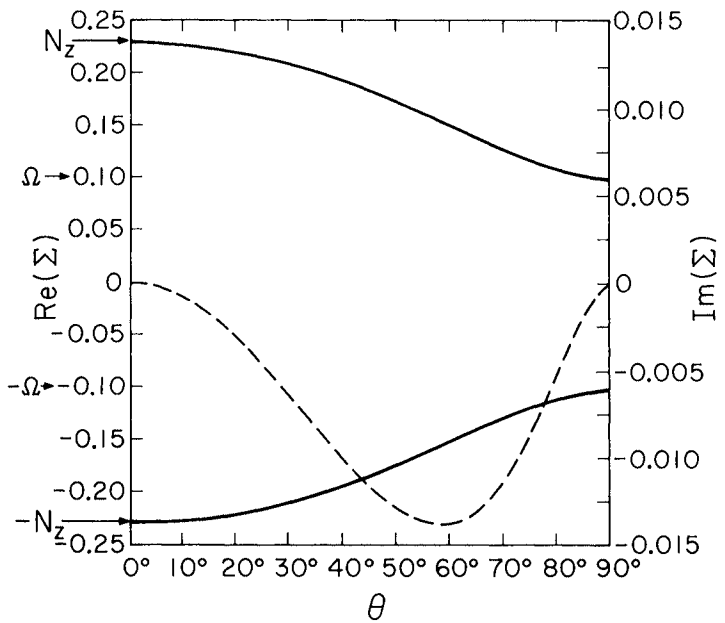

FIG. 6

FIG. 3.—The acoustic mode solutions of the quintic equation (4.3) evaluated at the "equatorial" point. The real part (*solid line*) and imaginary part (*dashed line*) of Σ (in rad s^{-1}) are functions of $\theta = \sin^{-1}(k_z/|\mathbf{k}|)$.

FIG. 4.—The acoustic mode solutions of the quintic equation (4.3) evaluated at the "surface" point; same notation as Fig. 3

FIG. 5.—The intermediate-frequency mode solutions of the quintic equation (4.3) evaluated at the "equatorial" point. These modes display the characteristics of both internal gravity waves and inertial waves; same notation as Fig. 3.

FIG. 6.—The intermediate-frequency mode solutions of the quintic equation (4.3) evaluated at the "surface" point; same notation as Fig. 3

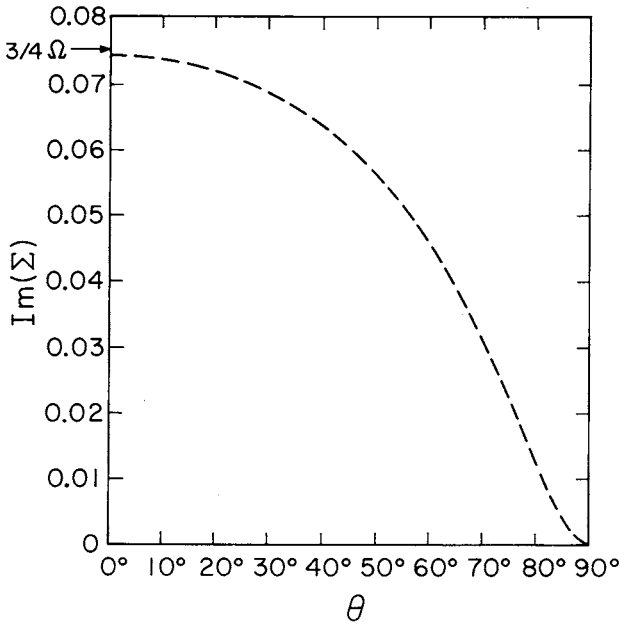

FIG. 7.—The "dynamical instability" (Σ purely imaginary) solution of the quintic equation (4.3) evaluated at the "surface" point; same notation as Fig. 3

For $L \ll S^3$, we have

$$\Sigma = \pm S + \frac{iL}{2S^2}, \tag{6.3}$$

showing that these are basically the longitudinal modes (acoustic waves). For Keplerian motion $\tilde{\omega}(\partial\Omega/\partial\tilde{\omega}) = -3\Omega/2$, and hence small perturbations grow fastest in the direction where $k_{\tilde{\omega}} = m/\tilde{\omega}, k_z = 0$ for which $Im(\Sigma) \geq -3\Omega/8$.

Equation (6.1) describes the behavior of an acoustic wave in a medium sheared by differential rotation. The leading terms, in fact, can be derived directly for sound waves propagating in a two dimensional pure shear without including rotation or cylindrical coordinates. At an arbitrary point P, we set up coordinates with x parallel to $\tilde{\omega}$, y parallel to ϕ, and z unchanged. Using the local description of a shearing rotation (Mihalas and Binney 1981, p. 472f.), one can show that the velocity near P is given by

$$\boldsymbol{v} = \Omega_P\{-y\hat{x} + [1 + (\partial \ln \Omega/\partial \ln \tilde{\omega})_P]x\hat{y}\}. \tag{6.4}$$

The pure shear component of this is (cf. § 2.3 of Batchelor 1967)

$$\boldsymbol{v} = \tfrac{1}{2}\tilde{\omega}\frac{\partial\Omega}{\partial\tilde{\omega}}(y\hat{x} + x\hat{y}). \tag{6.5}$$

In the vicinity of P, then, the linearized equations of motion for an homogeneous medium are

$$\frac{\partial v_x'}{\partial t} + v_x\frac{\partial v_x'}{\partial x} + v_y\frac{\partial v_x'}{\partial y} + v_x'\frac{\partial v_x}{\partial x} + v_y'\frac{\partial v_x}{\partial y} + \frac{c_s^2}{\rho}\frac{\partial \rho'}{\partial x} = 0, \tag{6.6}$$

$$\frac{\partial v_y'}{\partial t} + v_x\frac{\partial v_y'}{\partial x} + v_y\frac{\partial v_y'}{\partial y} + v_x'\frac{\partial v_y}{\partial x} + v_y'\frac{\partial v_y}{\partial y} + \frac{c_s^2}{\rho}\frac{\partial \rho'}{\partial y} = 0, \tag{6.7}$$

and the continuity equation is

$$\frac{\partial \rho'}{\partial t} + v_x\frac{\partial \rho'}{\partial x} + v_y\frac{\partial \rho'}{\partial y} + \rho\frac{\partial v_x'}{\partial x} + \rho\frac{\partial v_y'}{\partial y} = 0. \tag{6.8}$$

Introducing the assumption that all variables are proportional to $\exp[i(\sigma t + k_x x + k_y y)]$ leads to the matrix equation at P:

$$\begin{pmatrix} i\sigma & \frac{1}{2}\tilde{\omega}\frac{\partial\Omega}{\partial\tilde{\omega}} & ik_x c_s^2 \\ \frac{1}{2}\tilde{\omega}\frac{\partial\Omega}{\partial\tilde{\omega}} & i\sigma & ik_y c_s^2 \\ ik_x & ik_y & i\sigma \end{pmatrix}\begin{pmatrix} v_x' \\ v_y' \\ \frac{\rho'}{\rho} \end{pmatrix} = 0. \tag{6.9}$$

For a nontrivial solution, the determinant of the matrix must vanish; hence to leading order in S/Ω,

$$\sigma^3 - \sigma(k_x^2 + k_y^2)c_s^2 - ik_x k_y \tilde{\omega}(\partial\Omega/\partial\tilde{\omega})c_s^2 = 0 , \tag{6.10}$$

which is the same as equation (6.1). The unstable quadrants are those in which the shear flow at any point has a component toward P.

We emphasize that the existence of unstable modes in a local analysis does not necessarily imply a global instability.

VII. GLOBAL OSCILLATIONS: AN ESTIMATION

The observed DNOs and QPOs cannot be caused by *short*-wavelength oscillations of the white dwarf or the accretion disk; such oscillations simply could not be resolved by distant observers. Thus any serious comparison with the observed periods must involve a *global* analysis of the pulsation of the components of the dwarf novae, and as such must include a proper treatment of the boundary conditions. It is nevertheless tempting to stretch the limitations of our short-wavelength analysis by applying our results to the observations in hope of gaining some insight into the problem.

In this spirit, we (unjustifiably) allow $k_{\tilde{\omega}}\tilde{\omega}$, m, and $k_z z_{0.2}$ each to assume values of order unity in the quintic equation (4.3). This is admittedly a violation of the condition under which the quintic equation is valid, namely that the wavelength of the oscillation be small compared to any local scale length of the disk. However, we are encouraged by the success of a similar approximation for stellar pulsation. For the adiabatic oscillation of a nonrotating star, a local analysis yields a fourth-order equation analogous to the quintic equation (4.3). This equation may be written as (cf. § 14 of Unno *et al.* 1979, or § 17.10 of Cox 1980)

$$k^2 = -\left(\frac{S_l^2}{\sigma^2} - 1\right)\left(\frac{\sigma^2}{N^2} - 1\right)\frac{N^2}{c_s^2} . \tag{7.1}$$

Here, S_l^2 is the critical acoustic frequency

$$S_l^2 = \frac{l(l+1)}{r^2}\, c_s^2 , \tag{7.2}$$

where k is the radial wavenumber and l is an index of the spherical harmonic Y_l^m. (This is the separation of variables for stellar pulsation alluded to in § IV.)

For the long radial wavelengths (small k) appropriate to global oscillations, equation (7.1) gives

$$\sigma^2 \approx S_l^2, N^2 . \tag{7.3}$$

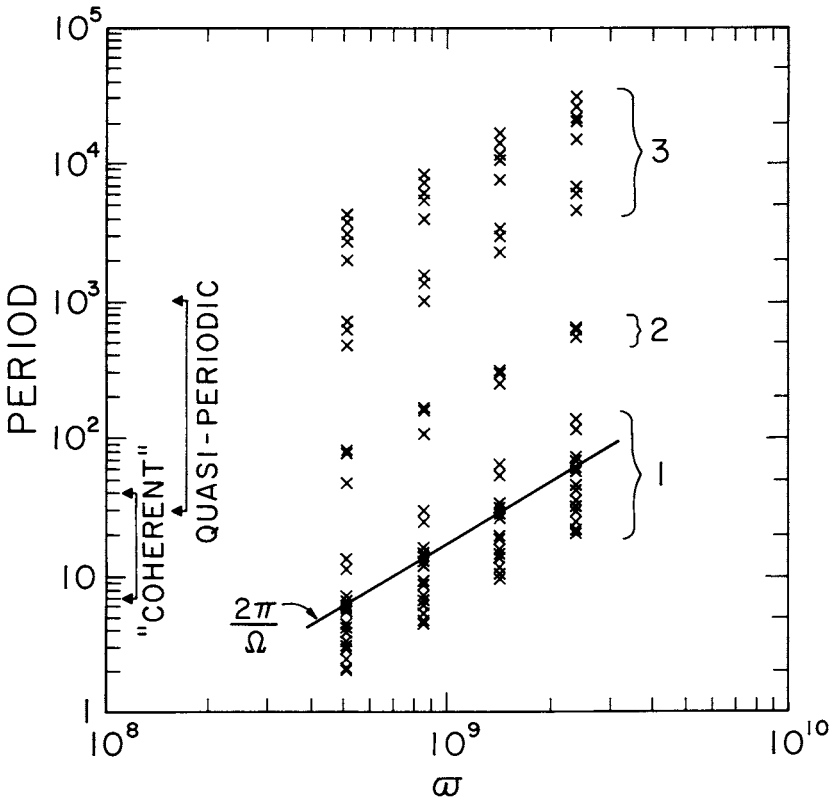

FIG. 8.—Oscillation period (s) plotted as a function of the cylindrical radius $\tilde{\omega}$ (cm) at four "intermediate" model points. Each cross indicates a solution of the quintic equation (4.3). The ranges of the observed "coherent" and quasi-periodic oscillation periods are indicated, as are the three period "bands" discussed in the text. Each band contains both stable and unstable modes of oscillation. No clear separation between stable and unstable modes is discernible. The local Keplerian rotation period ($=2\pi/\Omega$) is shown for comparison.

For simple stellar models, such as polytropes or zero-age main-sequence models, the oscillation frequencies obtained from a proper global analysis are quite comparable to approximate solutions given by equation (7.1) for a point deep in the interior of the star. It is our hope that the solution of the quintic equation (4.3) for a judiciously chosen point in the accretion disk model will similarly produce reasonable estimates of the global oscillation frequencies of the disk. To produce such estimates of the global disk oscillation frequencies, we have carried out our calculations for extended regions near the inner radius and equatorial plane of the disk. This should at least provide estimates of the ranges of frequencies in which the global oscillation frequencies fall. Specifically, we have evaluated the quintic equation at four radial positions, ranging from $\tilde{\omega}_1$, the inner radius of the disk, to $5\tilde{\omega}_1$, and equally spaced in log $\tilde{\omega}$.

For the vertical position, we have chosen an "intermediate" height of $z/z_{0.2} \approx 5.0 \times 10^{-2}$; this point is characterized by comparable values of $N_{\tilde{\omega}}$ and N_z, ensuring that the oscillations will reflect both the horizontal and vertical stratification of the disk. Although the pulsation periods do increase with increasing radius in the disk, they are relatively insensitive to the vertical height; nearly the same periods were obtained for points near the equatorial plane as those for the points chosen for our analysis.

To provide a variety of orientations of the wave vector $\boldsymbol{k}$, we consider all 26 nontrivial combinations: $k_{\tilde{\omega}}\tilde{\omega} = 0, 1, 2$; $m = 0, 1, 2$; and $k_z z_{0.2} = 0, 1, 2$. (The results are unchanged if negative values are included as well.) The frequencies obtained from the quintic equation (4.3) have been converted into the periods $P = 2\pi/(\Sigma - m\Omega)$, as would be observed from an inertial frame. The results are displayed in Figure 8.

The periods fall into three groups or "bands":

1. Small periods, with $2 \lesssim P \lesssim 140$ s, roughly of the order of the local Keplerian orbital period. This is not surprising; for small $|\boldsymbol{k}|$, $H_{\tilde{\omega}} \approx \Omega$ is the dominant frequency in the disk interior. This "band" overlaps the periods observed for the dwarf nova oscillations.
2. Intermediate periods, with $49 \lesssim P \lesssim 640$ s. These oscillations are a combination of retrograde $m = 1$ modes (see [3] below) and oscillations for which the waves propagate radially while the mass elements move vertically, as seen in § V for internal gravity waves. (However, $|\sigma|/N_z \approx 0.4$ for the latter modes, while $|\sigma| = N_z$ for the short-wavelength gravity wave solutions.) This range of periods coincides with that observed for the quasi-periodic oscillations of dwarf novae.
3. Large periods, with $P \gtrsim 480$ s. All these oscillations are retrograde waves with $m = 1$, traveling in a direction opposite the Keplerian orbital velocity with (corotating) frequency $\Sigma \approx \Omega$. (The corresponding prograde modes reside in the previous two "bands.") Thus, in an inertial frame, the frequency $\sigma = \Sigma - m\Omega \approx 0$, resulting in a large period.

While the overlapping of the ranges of the small and intermediate period "bands" with the observed periods of the "coherent" and quasi-periodic oscillations is encouraging and suggestive, it remains to be seen whether this can be confirmed by a more rigorous investigation. Nevertheless, the results indicate the importance of including the effects of the vertical stratification of the disk and underscore the desirability of a global analysis, with its proper treatment of the relevant boundary conditions. Only then can meaningful comparisons be made with the observed oscillations.

We wish to thank Dr. Carl J. Hansen for several helpful comments. This work has been supported in part by National Science Foundation grant AST83-07214 through the University of Rochester.

REFERENCES

Abramowicz, M. A., Livio, M., Piran, T., and Wiita, P. J. 1984, *Ap. J.*, **279**, 367.
Batchelor, G. K. 1967, *An Introduction to Fluid Mechanics* (Cambridge: Cambridge University Press).
Cabot, W. 1982, Ph.D. thesis, University of Rochester.
Cordova, F. A., and Mason, K. O. 1982, in *Pulsations in Classical and Cataclysmic Variable Stars*, ed. J. P. Cox and C. J. Hansen (Boulder: Joint Institute for Laboratory Astrophysics, University of Colorado), p. 23.
Cox, J. P. 1980, *Theory of Stellar Pulsation* (Princeton: Princeton University Press).
———. 1981, *Ap. J.*, **247**, 1070.
Cox, J. P., and Everson, B. L. 1982, in *Pulsations in Classical and Cataclysmic Variable Stars*, ed. J. P. Cox and C. J. Hansen (Boulder: Joint Institute for Laboratory Astrophysics, University of Colorado), p. 42.
Kato, S. 1978, *M.N.R.A.S.*, **185**, 629.
Kato, S. 1983, *Pub. Astr. Soc. Japan*, **35**, 249.
Livio, M., and Shaviv, G. 1981, *Ap. J.*, **244**, 290.
Mihalas, D., and Binney, J. 1981, *Galactic Astronomy* (2d ed.; San Francisco: W. H. Freeman).
Patterson, J. 1981, *Ap. J. Suppl.*, **45**, 517.
Pringle, J. E. 1981, *Ann. Rev. Astr. Ap.*, **19**, 137.
Robinson, E. L., and Nather, R. E. 1979, *Ap. J. Suppl.*, **39**, 461.
Tassoul, J.-L. 1978, *Theory of Rotating Stars* (Princeton: Princeton University Press).
Unno, W., Osaki, Y., Ando, H., and Shibahashi, H. 1979, *Nonradial Oscillations of Stars* (Tokyo: University of Tokyo Press).
Van Horn, H. M., Wesemael, F., and Winget, D. E. 1980, *Ap. J. (Letters)*, **235**, L143.

WILLIAM CABOT: Goddard Institute for Space Studies, 2880 Broadway, New York, NY 10025

BRADLEY W. CARROLL, PATRICK N. MCDERMOTT, MALCOLM P. SAVEDOFF, and HUGH M. VAN HORN: Department of Physics and Astronomy, University of Rochester, Rochester, NY 14627